Tracing the Light— Introduction to the Mathematics of BioLuminescence Tomography

Yang Yang

1. BioLuminescence Tomography

On a tranquil summer night, the air carries the sweet fragrance of blooming flowers, mingled with the soft rustle of grass in a meadow. The moonlight casts a gentle glow, illuminating the serene ambiance. Amidst this nocturnal scene, fireflies are dancing and playing. These tiny, luminous creatures orchestrate a mesmerizing spectacle, transforming the darkness into an ethereal glow.

This natural light show has captivated the imagination of poets and writers for its aesthetic beauty in various literary works. Interestingly, the phenomenon goes beyond aesthetics. The principle behind fireflies' illumination has inspired researchers to harness and manipulate this natural phenomenon for scientific benefits. The idea has led to the development of a cutting-edge technology in biomedical imaging known as *BioLuminescence Tomography (BLT)*.

Bioluminescence is the process of light emission in living organisms. The phenomenon occurs widely in nature, with typical examples including fireflies, jellyfish, and certain types of fungi (Figure 1). These creatures illuminate as they carry DNA that encodes luminescent proteins, and these proteins emit visible light when they undergo specific biochemical reactions. In 2018, the Nobel Prize in Chemistry was awarded to three researchers: Osamu Shimomura, Martin Chalfie, and Roger Tsien for their discovery and development of a glowing jellyfish protein known as the green fluorescent protein. The green light has since played crucial roles in biomedical research, enabling scientists to track how cancer tumors form new blood vessels,

Yang Yang is an associate professor in the Department of Computational Mathematics, Science, and Engineering at Michigan State University. His email address is yangy5@msu.edu.

Communicated by Notices Associate Editor Reza Malek-Madani. For permission to reprint this article, please contact: reprint-permission@ams.org.

DOI: https://doi.org/10.1090/noti3051

how Alzheimer's disease kills brain neurons, and how HIV-infected cells produce new viruses.





Figure 1. Bioluminescent organisms: (a) Fireflies. (b) Jellyfish.

The term "tomography" is derived from the Greek words *tomos* meaning "slice" or "section," and *graphia* meaning "writing" or "drawing." Tomography is an imaging technique that enables non-destructive visualization of objects by acquiring cross-sectional images. In a tomographic imaging process, the object is positioned within an imaging device that can capture multiple cross-sectional images of the object from different angles. These images are processed by computers to reconstruct three-dimensional representations of the internal structures.

BLT operates on the fundamental idea of utilizing bioluminescent sources to trace and visualize biological processes at the cellular level. Bioluminescent sources are typically cells that have been genetically engineered to express bioluminescent proteins. In a BLT experiment, researchers inject bioluminescent sources into biological tissue. Following the injection, the tissue is placed in a dark environment to minimize external light interference. Optical detectors or cameras are positioned around to capture the bioluminescent light emitted from within. When the sources are excited, they undergo biochemical reactions and illuminate. The light illumination is recorded by the optical detectors and utilized for computing the spatial

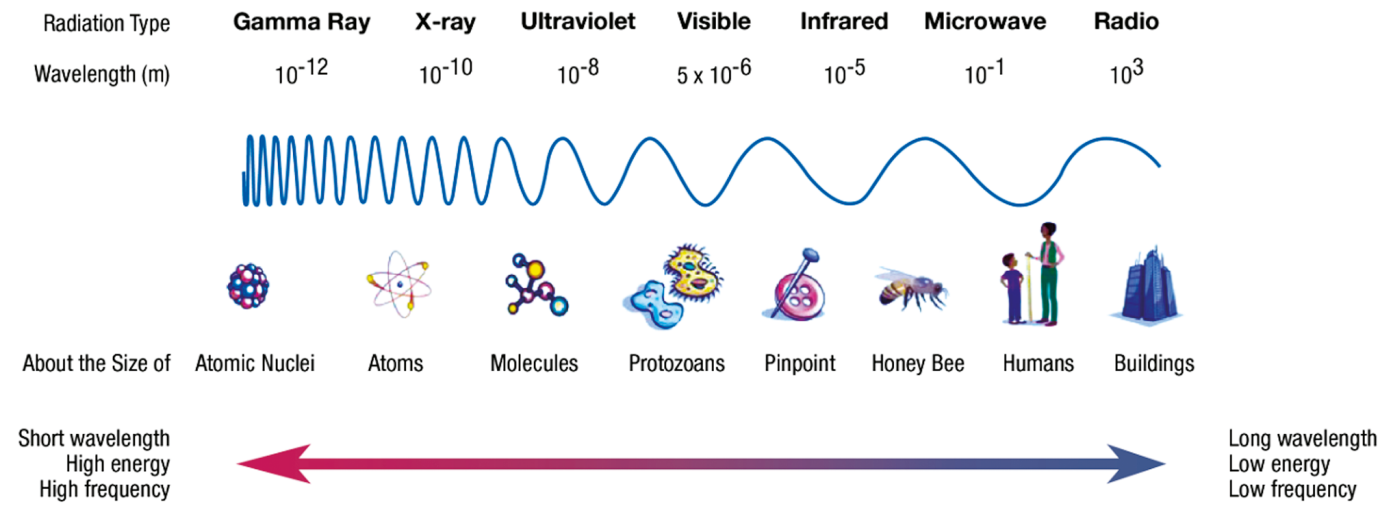


Figure 2. The electromagnetic spectrum.

distribution of the bioluminescence source. The distribution serves as effective biomarkers for biological processes of interest. BLT shows significant potential in the context of cancer diagnostics: By introducing bioluminescent sources specific to cancer cells, this technology enables dynamic imaging to monitor the progression of malignant cells.

This introductory essay endeavors to guide readers through some fascinating mathematics within BLT. The focus lies on formulating the problems and outlining key ideas for their solution without delving into technical details. The exploration encompasses modeling light propagation in biological tissue using an integrodifferential equation in Section 2, analyzing the well-posedness of the forward modeling in Section 3, investigating inverse problems arising in the imaging process of BLT in Section 4, as well as discussing several related contemporary research areas in Section 5.

2. Light Propagation in Biological Tissue

The illumination utilized in BLT generally falls within the visible light spectrum. Visible light is a narrow band of the entire electromagnetic (EM) spectrum. EM radiation is a form of energy that travels through space in the form of waves. Examples include radio wave, microwave, visible light, X-ray, and gamma ray (Fig. 2). The elementary particles of EM radiation are *photons*. Each photon carries energy that is inversely proportional to the wavelength of the EM radiation, with shorter wavelengths corresponding to higher photon energy (Fig. 2). Photons interact with biological tissue primarily through two processes: absorption and scattering (Fig. 3).

Absorption is the process in which photons are absorbed by atoms, molecules, or particles in a medium. The absorbed photons elevate electrons in the absorber from ground states to excited states. In the meanwhile, loss of

photons causes graduatal reduction of the intensity of EM radiation as it propagates in the medium. A medium's ability to absorb photons is quantitatively characterized by its absorption coefficient α , which is defined as the probability of photon absorption per unit path length. The representative value of α in biological tissue is 0.1 cm⁻¹ [WW12]. The reciprocal α^{-1} is known as the absorption mean free path.

Scattering is the process in which photons change the direction of propagation after interacting with small particles in a medium. The amount of scattering depends on wavelength of the EM radiation as well as size and structure of the medium. Scattering redirects photons, causing a diffused spread of EM radiation. A medium's ability to scatter photons is quantitatively characterized by its *scattering coefficient* σ , which is defined as the probability of photon scattering per unit path pength. The representative value of σ in biological tissue is 100 cm^{-1} [WW12]. The reciprocal σ^{-1} is known as the *scattering mean free path*.

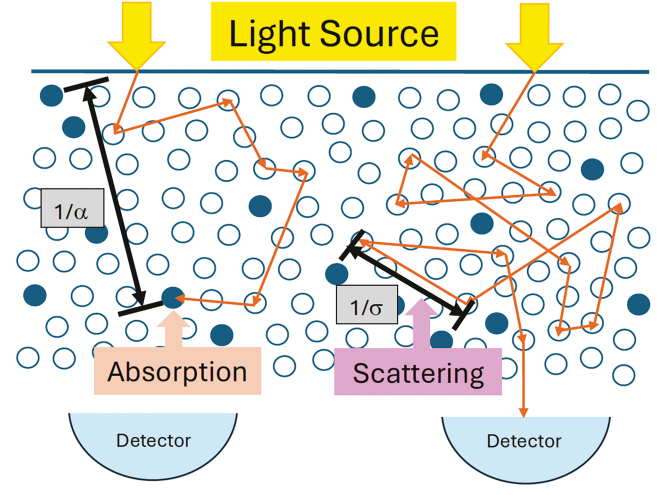


Figure 3. Light absorption and scattering.

2.1. Radiative Transfer Equation. We henceforth denote biological tissue by a bounded open convex subset $\Omega \subset \mathbb{R}^n$ with smooth boundary $\partial\Omega$. The dimensions of practical significance are n=2 (2D) and n=3 (3D), but the mathematical framework works equally well in other dimensions.

The fundamental quantity for light propagation is *radiance*, defined as the photon energy per unit normal area per unit solid angle. It is a measure of the photon intensity at a point in a particular direction. The distribution of radiance is generally dynamic as photons propagate. However, the processes of interest in BLT typically evolve on timescales much longer than the rapid propagation of light. It is thus valid to simply consider a stationary distribution of radiance. We denote the radiance at $x \in \Omega$ in the direction $\theta \in \mathbb{S}^{n-1}$ by $u(x,\theta)$, where \mathbb{S}^{n-1} is the (n-1)-dimensional unit sphere. As a result, the rate of change of the radiance in the θ -direction is naturally modeled by the directional derivative $\theta \cdot \nabla u$ where $\nabla = \nabla_x$ is the spatial gradient.

The variation in radiance at x in a particular direction θ primarily results from three factors: 1. loss of photons by absorption and scattering; 2. gain of photons by scattering; and 3. gain of photons by bioluminescent emission. These effects are modeled as follows: 1. Loss of photons by absorption and scattering is proportional to the photon density, with the proportional factors $\alpha(x)$ and $\sigma(x)$, respectively. If we write $a := \alpha + \sigma$, then the total loss is $-a(x)u(x,\theta)$. 2. Gain of photons by scattering is proportional to the photon density that is scattered to the direction θ from other directions. Let $k(x, \theta, \theta')$ be the probability of photons in the θ' -direction being scattered to the θ -direction, then the gain of photons due to scattering is $\sigma(x) \int_{\mathbb{S}^{n-1}} k(x, \theta, \theta') u(x, \theta') d\theta'$ where $d\theta'$ is the (normalized) spherical measure on \mathbb{S}^{n-1} . 3. Gain of photons by bioluminescent emission is due to the presence of the bioluminescent source f(x). All these factors combined lead to the following Radiative Transfer Equation (RTE) on $\Omega \times \mathbb{S}^{n-1}$ that dictates light propagation in biological tis-

$$\theta \cdot \nabla u(x,\theta) + a(x)u(x,\theta) - \sigma(x) \int_{\mathbb{S}^{n-1}} k(x,\theta,\theta')u(x,\theta') d\theta' = f(x).$$
 (1)

Here $k(x, \theta, \theta')$ is known as the *scattering kernel*. As a probability density function, it is non-negative and satisfies $\int_{\mathbb{S}^{n-1}} k(x, \theta, \theta') d\theta' = \int_{\mathbb{S}^{n-1}} k(x, \theta, \theta') d\theta = 1$. We will refer to α, σ, k as *optical parameters*. These parameters along with the bioluminescent source f are allowed to be spatially varying (that is, x-dependent) in the model to capture inhomogeneity of the medium. In applications, the following spatially-invariant Henyey-Greenstein scattering kernel has proven to be useful in approximating the an-

gular scattering dependence of single scattering events in biological tissue:

$$k_{HG}(x,\theta,\theta') := \begin{cases} \frac{1}{2\pi} \frac{1-g^2}{1+g^2 - 2g(\theta \cdot \theta')} & \text{in } 2D\\ \frac{1}{4\pi} \frac{1-g^2}{\left[1+g^2 - 2g(\theta \cdot \theta')\right]^{\frac{3}{2}}} & \text{in } 3D, \end{cases}$$

where the constant $g \in (-1,1)$ is a measure of anisotropy, with g = 0 corresponding to isotropic scattering.

2.2. Boundary condition. In BLT, the bioluminescent sources are cells that have been genetically engineered to express bioluminescent proteins. No external light source is imposed to prevent contamination of the internal light source. As a result, there is no radiance flowing into the tissue from the boundary. Note that the RTE holds on $\Omega \times \mathbb{S}^{n-1}$ whose boundary $\partial \Omega \times \mathbb{S}^{n-1}$ is the union of two subsets $\Gamma_{\pm} := \{(x, \theta) \in \partial \Omega \times \mathbb{S}^{n-1} : \pm \nu(x) \cdot \theta \geq 0\}$ with ν the unit outer normal vector field on $\partial \Omega$. The subset Γ_{+} consists of the outward-pointing directions on the boundary, while Γ_{-} consists of the inward-pointing directions on the boundary and *incoming boundary*, respectively. The fact that no radiance flows into the tissue translates to the boundary condition

$$u|_{\Gamma} = 0. (2)$$

3. The Forward Problem and Structure of Solutions

The RTE provides a mathematical framework for understanding light propagation in biological tissue. In particular, if all the optical parameters α , σ , k as well as the bioluminescent source f are specified, the distribution of the radiance is characterized by the solution of the boundary

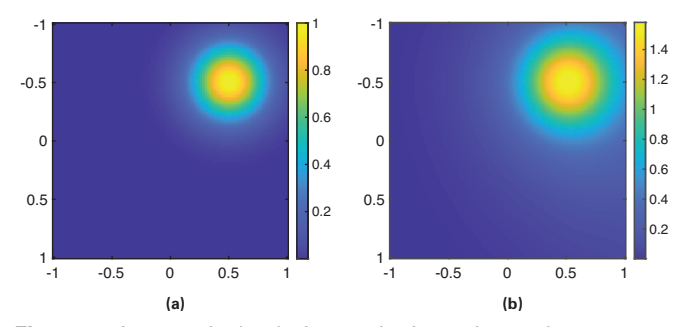


Figure 4. A numerical solution to the boundary value problem (1) (2) on the 2D unit square $\Omega=[-1,1]\times[-1,1]$. Here, $a(x_1,x_2)\coloneqq 3-2x_1$, $\sigma(x_1,x_2)=1$, and the 2D Henyey-Greenstein scattering kernel k_{HG} with g=0.5. (a) bioluminescent source $f(x_1,x_2)=e^{-10(x_1-\frac{1}{2})^2-10(x_2+\frac{1}{2})^2}$. (b) Angularly averaged RTE solution $\int_{\mathbb{S}^1}u(x_1,x_2,\theta)\,d\theta$. The angular averaging is applied for the ease of illustration, as the graph of the RTE solution $u(x_1,x_2,\theta)$ is 4D and cannot be represented by a colored image.

value problem (1) (2). In this section, we derive this solution and investigate its structure.

Introduce

$$\begin{split} T_a u(x,\theta) &:= (\theta \cdot \nabla + a(x)) u(x,\theta), \\ K u(x,\theta) &:= \sigma(x) \int_{\mathbb{S}^{n-1}} k(x,\theta,\theta') u(x,\theta') \, d\theta'. \end{split}$$

Here K is an integral operator, and T_a is a first-order linear differential operator equipped with the domain $D(T_a) := \{u \in L^2(\Omega \times \mathbb{S}^{n-1}) : \theta \cdot \nabla u \in L^2(\Omega \times \mathbb{S}^{n-1}), u|_{\Gamma_-} = 0\}$. Using these notations, the boundary value problem (1) (2) can be written in the operator form:

$$(T_a - K)u = f, \qquad u \in D(T_a). \tag{3}$$

Therefore, solving for the RTE solution u amounts to inverting the operator $T_a - K$ on $D(T_a)$.

3.1. Non-scattering media. When photon scattering in a medium is relatively weak, we can neglect the scattering effect by taking $\sigma = 0$ and simply concentrate on photon absorption. Such a medium is referred to as nonscattering. Negligible scattering usually occurs when the radiation wavelength is sufficiently short, or equivalently, when the photon energy is sufficiently high. This is not the case in BLT though: visible light photons in BLT do not carry enough energy and typically exhibit strong scattering in biological tissue. As such, biological tissue cannot be regarded as a non-scattering medium for visible light. However, there are still good reasons to begin with the non-scattering assumption. On the one hand, it provides an important intermediate step toward understanding the full structure of RTE solutions. On the other hand, there do exist modalities that make use of EM radiation with sufficiently short wavelengths for medical imaging in biological tissue (and they are probably better known to the public than BLT), such as Computed Tomography and Single Photon Emission Computed Tomography. Understanding non-scattering scenarios will provide insight into the mathematical mechanisms of these imaging modalities.

In a non-scattering medium, we have $\sigma=0$ hence K=0. The operator form (3) simplifies to $T_au=f$. This is a first-order linear partial differential equation. The solution subject to $u|_{\Gamma_-}=0$ can be found using the method of characteristics:

$$T_a^{-1}f(x,\theta) := \int_{-\tau_-(x,\theta)}^0 e^{\int_{-t}^0 a(x+s\theta)\,ds} f(x+t\theta)\,dt \qquad (4)$$
$$(x,\theta) \in \Omega \times \mathbb{S}^{n-1}$$

where $\tau_{\pm}(x,\theta) > 0$ is defined so that $(x, x \pm \tau_{\pm}(x,\theta)\theta) \in \Gamma_{\pm}$. This representation indicates that the radiance at x in the θ -direction is attributed to the photons travel-

ing in the straight line segment $\ell_{x,\theta} := \{(x + t\theta, \theta) : t \in [-\tau_{-}(x,\theta), \tau_{+}(x,\theta)]\}$ with the exponential attenuation $e^{\int_{-t}^{0} a(x+s\theta) ds}$, see Fig. 5.

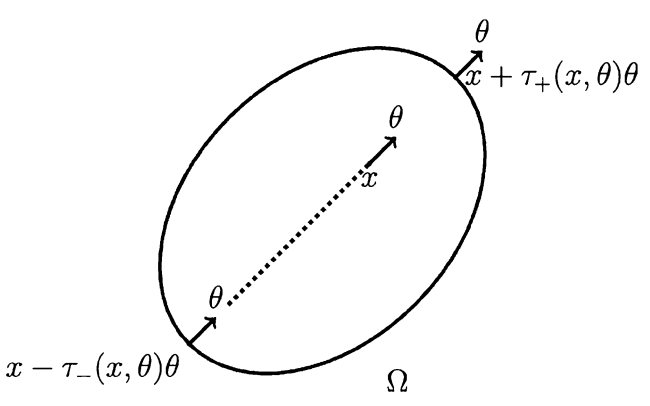


Figure 5. Definition of $\tau_{\pm}(x,\theta)$. The dotted line represents photon trajectories that contribute to the radiance at x in the θ -direction in the absence of scattering.

3.2. Scattering medium. The calculation above shows that T_a is invertible on the domain $D(T_a)$ and $T_a^{-1}f$ is given by (4). Therefore, in a scattering medium where $\sigma \neq 0$, the operator form (3) is equivalent to the integral equation

$$(I - T_a^{-1}K)u = T_a^{-1}f, \qquad u \in D(T_a).$$
 (5)

where I is the identity operator. This integral representation turns out to be informative in the analysis of RTE solutions. In particular, it suggests that we may view $T_a^{-1}K$ as a perturbation to the identity operator. For instance, suppose the absorption and scattering coefficients are suitable so that $T_a^{-1}K$ is a contraction (that is, $||T_a^{-1}K|| < 1$ with respect to a suitable norm $||\cdot||$), then $I - T_a^{-1}K$ is invertible with a bounded inverse, and the solution is represented by the following Neumann series:

$$u = (I - T_a^{-1}K)^{-1}T_a^{-1}f$$

= $(I + T_a^{-1}K + T_a^{-1}KT_a^{-1}K + \cdots)T_a^{-1}f.$ (6)

This representation immediately implies that the integral equation (5) admits a unique solution, and the solution depends continuously on the source f. The assumptions to make $T_a^{-1}K$ a contraction usually involve conditions on the relative order of magnitude of α and σ , known as the *sub-critical conditions* [Ago98, CS99]. This series solution reveals that the radiance at x in the θ -direction comes from infinite terms. Let us look at them one by one. The first term, $T_a^{-1}f(x,\theta)$, as we have discussed in the previous subsection, represents the photons that travel in a straight line and arrive at x in the θ -direction without undergoing scattering interactions. From the second term onward, the scattering operator K appears, indicating the involvement of scattering. The second term $T_a^{-1}KT_a^{-1}f(x,\theta)$ represents the particles that are bounced to x in the θ -direction after

undergoing a single scattering interaction. Likewise, the general term $(T_a^{-1}K)^nT_a^{-1}f(x,\theta)$ represents the photons that are bounced to x in the θ -direction after undergoing n scattering interactions. Consequently, the total radiance at x in the θ -direction is the sum of photons arriving from various locations along different paths (Fig. 6).

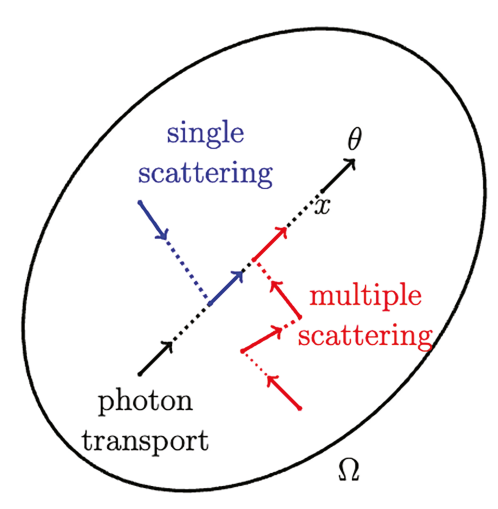


Figure 6. Selected photon trajectories in the presence of scattering. The black/blue/red dotted lines represent photon trajectories that experience no/single/multiple scattering before contributing to the radiance at x in the θ -direction.

4. The Inverse Problem and Integral Transforms

Given the optical parameters α , σ , k as well as the bioluminescent source f, the analysis in Section 3 shows that the distribution of radiance is determined by the Neumann series representation (6). However, the bioluminescent source f is not known in BLT. Instead, it is this source that serves as biomarkers of biological processes and must be computed for the imaging purpose. What one can measure in BLT is the radiance that flows out of the tissue and captured by optical cameras. If we consider the idealized scenario where optical cameras are placed everywhere around the tissue and denote by $R_+u \coloneqq u|_{\Gamma_+}$ the restriction operator onto the outgoing boundary (in the trace sense), then the BLT data, in view of (6), is

$$\mathcal{X}_{a,\sigma}f := u|_{\Gamma_+} = R_+ (I - T_a^{-1}K)^{-1} T_a^{-1} f. \tag{7}$$

The operator $\mathcal{X}_{a,\sigma}$ maps the unknown source linearly to the data and is referred to as the *source-to-data map*. As a result, the imaging problem in BLT can be mathematically formulated as inverting the source-to-data map. This type of problem, where the goal is to recover the cause (i.e., the bioluminescent source) from an observed effect (i.e., the outgoing radiance), is common in science and engineering. Such problems are known as *inverse problems*, in contrast to "forward problems" where the cause is given and the task is to simulate or predict observations. For example, solv-

ing the RTE boundary value problem with specified optical coefficients and bioluminescent sources, as discussed in Section 3, is a forward problem. This section focuses on the inverse problem in BLT. Along the journey of investigation, we will make brief detours to explore mathematical models for a few other notable medical imaging methods. These models, which can be viewed as simplified versions of the BLT model, hold both practical significance and mathematical interest on their own. Throughout this section, we assume the optical parameters α , σ , k are known, and the objective is to invert the source-to-data map $\mathcal{X}_{a,k}$.

4.1. Non-scattering media.

Non-absorbing non-scattering media. Let us begin with the idealized scenario where neither absorption nor scattering occurs, that is $\alpha = \sigma = 0$. Then K = 0 and the source-to-data map (7) reduces to:

$$\begin{split} \mathcal{X}_{0,0}f(x,\theta) &\coloneqq R_+ T_0^{-1}f(x,\theta) \\ &= \int_{-\tau_-(x,\theta)}^0 f(x+t\theta)\,dt, \quad (x,\theta) \in \Gamma_+. \end{split}$$

Here $(x,\theta) \in \Gamma_+$ can be identified with the line segment $\ell_{x,\theta}$ so that Γ_+ provides a parameterization of all the line segments inside Ω , see Fig. 7. If we extend f to be a function in \mathbb{R}^n that vanishes outside Ω and denote this extension again by f, the source-to-data map $\mathcal{X}_{0,0}$ defines an integral transform that maps the function f to its line integrals, known as the X-ray transform. The inverse problem in BLT in a non-absorbing, non-scattering medium reduces to inverting the X-ray transform.

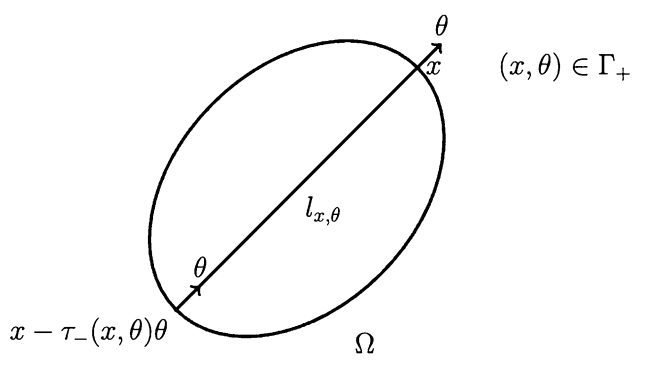


Figure 7. The line of integration in the definition of $\mathcal{X}_{0,0}$. Note that $(x,\theta) \in \Gamma_{+}$.

The term "X-ray transform" might seem strange in the context of BLT, where no X-rays are involved. Indeed, this name originates from another medical imaging modality *Computed Tomography*, or simply CT. CT images biological tissue utilizing X-rays, a type of EM radiation with wavelength in the range of 0.01 – 10 nanometers. (Fig. 2). Such wavelengths are significantly shorter compared to

visible light, allowing X-ray photons to carry considerably higher energy than light photons—so high that they experience negligible scattering in biological tissue (accounting for the assumption $\sigma = 0$) and travel along straight trajectories. In a CT scan, X-ray beams are directed from various angles through the body, and the transmitted Xray intensities are measured by detectors. The CT data is the difference between the outgoing X-ray intensities and the incoming X-ray intensities, known as the sinogram, see Fig. 8(b) for an example. Given that the drop in X-ray intensities is solely attributed to absorption, the sinogram consists precisely of line integrals of the absorption coefficient α along various straight trajectories, which is $\mathcal{X}_{0,0}\alpha$ using our notation. The imaging problem at the core of CT is the inverse problem of inverting the X-ray transform to recover the spatial distribution of α . This inverse problem was first studied in 2D by the Austrian mathematician Johann Radon (1887-1956). For this reason, the X-ray transform in 2D is also known as the Radon transform.1 Radon's investigation of the inverse problem was earlier than the invention of CT scanners and was mostly driven by mathematical considerations. Nevertheless, his mathematics turns out to play a crucial role in the theory of CT imaging. Interested readers are referred to the monographs [Eps08, Nat01] for in-depth discussion of the mathematics behind CT. The invention of CT has revolutionized medical diagnostics by providing detailed 3D images of internal structures, greatly improving the accuracy of diagnosis and treatment planning. Its societal benefits were recognized with the 1901 Nobel Prize in Physics awarded to the German physicist Wilhelm Röntgen for his discovery of X-rays, as well as the 1972 Nobel Prize in Physiology or Medicine that was awarded to the South African-American physicist Allen Cormack and the British engineer Sir Godfrey Hounsfield for their contribution to the development of CT scanners.

We sketch the idea to invert the X-ray transform. First, it is easy to show using the Cauchy-Schwarz inequality that $\mathcal{X}_{0,0}:L^2(\mathbb{R}^n)\to L^2(\Sigma,d\sigma)$ is a bounded linear operator. Here $\Sigma:=\{(z,\theta):\theta\in\mathbb{S}^{n-1},z\in\theta^\perp\}$ is a parameterization of lines and θ^\perp is the hyperplane orthogonal to θ , the measure $d\sigma=dS(z)d\theta$ where dS(z) is the usual Lebesgue measure on θ^\perp and $d\theta$ is the spherical measure on \mathbb{S}^{n-1} . As such, the X-ray transform has an adjoint $\mathcal{X}_{0,0}^*$ defined as

$$\begin{split} \mathcal{X}_{0,0}^*h(x) &\coloneqq \int_{\mathbb{S}^{n-1}} h(x-(x\cdot\theta)\theta,\theta)\,d\theta \\ &= \int_{\mathbb{S}^{n-1}} h(\ell_{x,\theta})\,d\theta \quad h = h(z,\theta) \in L^2(\Sigma,d\sigma). \end{split}$$

In words, h is a function that assigns values to each line $\ell_{x,\theta}$, and $\mathcal{X}_{0,0}^*h(x)$ is the average of h over all the lines that pass through x. For this reason, $\mathcal{X}_{0,0}^*$ is named the *back-projection*.

Now that we have two operators: $\mathcal{X}_{0,0}$ integrates over lines and $\mathcal{X}_{0,0}^*$ averages over lines, it seems a natural attempt to simply back-project the line integrals to hopefully recover something about the function. Direct calculation shows $\widehat{\mathcal{X}_{0,0}^*\mathcal{X}_{0,0}}f(\xi)=2\pi|\mathbb{S}^{n-2}||\xi|^{-1}\widehat{f}(\xi)$ in the Fourier domain where $\widehat{\cdot}$ denotes the Fourier transform and $|\mathbb{S}^{n-2}|$ is the surface area of \mathbb{S}^{n-2} . This relation suggests that \widehat{f} can be recovered if an extra Fourier multiplier is included to eliminate $|\xi|^{-1}$, leading to the following inversion formula:

$$f = \frac{1}{2\pi |\mathbb{S}^{n-2}|} \mathcal{X}_{0,0}^* \sqrt{-\Delta_z} \mathcal{X}_{0,0} f,$$

where $\sqrt{-\Delta_z}$ is the square root of the negative Laplacian in z. In 2D, one can further apply the relation $\sqrt{-\Delta_z} = H_z \frac{d}{dz}$ where H_z is the Hilbert transform with respect to the z variable to obtain

$$f = \frac{1}{4\pi} \mathcal{X}_{0,0}^* H_z \frac{d}{dz} \mathcal{X}_{0,0} f.$$

This is the inversion formula obtained by Radon. From the perspective of signal processing, the operator $H_z \frac{d}{dz}$ contributes $|\xi|$ in the Fourier domain and plays the role of a filter, thus the inversion formula filters the Radon transform before applying the back-projection. For this reason, the inversion is known as the *filtered back-projection*.

This filtering process includes the differentiation $\frac{d}{dz}$ which amplifies high-frequency content of the data. Such a filter generally makes functions more singular and sharpens blurred edges in images, see Fig. 8(c)(d). However, this feature raises significant issues when the data contains noise. Noise, which is of high frequency and non-differentiable, tends to be amplified during the inversion. As a result, even a small amount of noise in the data can lead to substantial deviations from the true source. In other words, the problem of inverting the Radon transform is *ill-posed*, meaning that the solution f is not continuously dependent on the data $\mathcal{X}_{0,0}f$. This issue essentially stems from the fact that the inverse Radon transform $\mathcal{X}_{0,0}^{-1}$ is an unbounded operator.

Absorbing non-scattering media. This case corresponds to $\sigma = 0$ hence $K \equiv 0$. The source-to-data map in view of (7) becomes

$$\begin{split} \mathcal{X}_{a,0}f(x,\theta) &\coloneqq R_+ T_a^{-1}f & (x,\theta) \in \Gamma_+ \\ &= \int_{-\tau_-(x,\theta)}^0 e^{\int_{-t}^0 a(x+s\theta)\,ds} f(x+t\theta)\,dt. \end{split}$$

This gives rise to another integral transform $\mathcal{X}_{a,0}$ that maps a function to its exponentially-attenuated line integrals,

¹The definitions of these two transforms diverge in 3D or higher dimensions, where the X-ray transform refers to integration over lines while the Radon transform refers to integration over hyperplanes.

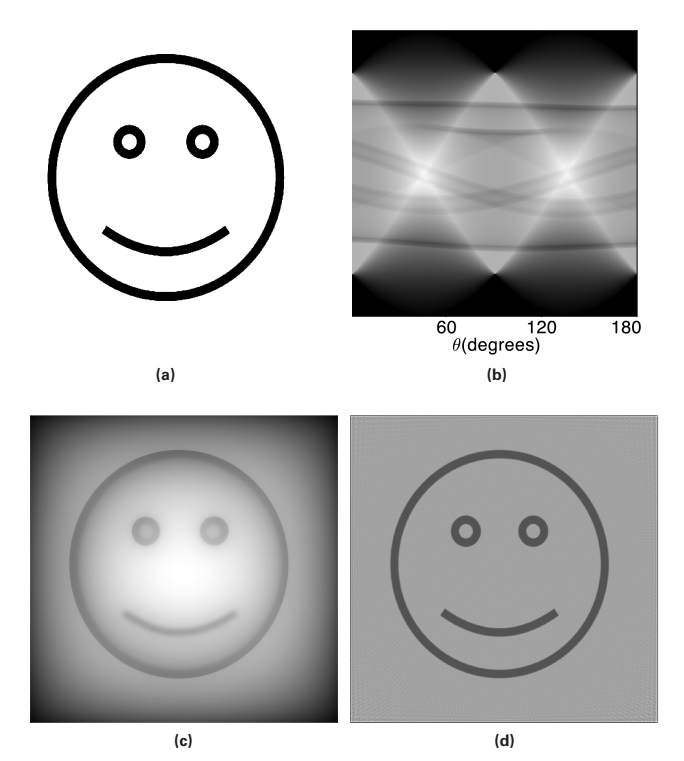


Figure 8. Numerical inversion of the X-ray transform $\mathcal{X}_{0,0}$: (a) Bioluminescent source f. (b) Sinogram $\mathcal{X}_{0,0}f$. (c) Back-projection $\mathcal{X}_{0,0}^*\mathcal{X}_{0,0}f$. (d) Filtered back-projection inversion.

known as the *attenuated X-ray transform*. The BLT inverse problem in an absorbing, non-scattering medium thus requires inversion of the attenuated X-ray transform.

This inverse problem, although motivated by the discussion of BLT here, rises earlier in another medical imaging modality Single Photon Emission Computed Tomography (SPECT). In SPECT, small doses of radioactive tracers that are able to emit single photons (e.g., Xenon-133) are injected into patients. The choice of the tracers depends on the specific organ or function being studied. These tracers accumulate in target tissues and emit gamma rays as they undergo radioactive decay. The detectors are rotated around the tissue to record the outgoing gamma rays. This data is then processed to create cross-sectional images of the distribution of the tracers. The spatial distribution of the gamma-ray radiance in SPECT can be effectively modeled by the same RTE (1) and the boundary condition (2), where the internal source f denotes the distribution of the radioactive tracers. As gamma rays carry even higher energy than X-rays (Fig. 2), the scattering effect again becomes negligible. Consequently, the inverse problem in SPECT is the same as that in BLT but with $\sigma = 0$. When implementing SPECT scans, CT scans are usually performed beforehand to obtain the attenuation coefficient α . It remains to invert the attenuated X-ray transform to image f.

Inversion of the attenuated X-ray transform presents greater challenges compared to its counterpart for the classical X-ray transform. In particular, the inversion formula must account for the exponential decay of X-ray intensity. Various inversion formulae have been derived in the literature by building insightful connections with other mathematical theories. Notably, [ABK97] reduces the inversion process in 2D to the boundary value problem for an elliptic equation with operator coefficients, developing the theory of A-analytic functions; [Nov02] adapts spectral analysis for eigenvalue equations [FS05] and connects the inversion with the inverse scattering theory for the RTE. As for the X-ray transform, the inversion of the attenuated X-ray transform is ill-pose in the sense that the inverse operator $\mathcal{X}_{a,0}^{-1}$ exists but is unbounded.

4.2. Scattering media. We are ready to invert the full source-to-data map $\mathcal{X}_{a,\sigma}$ in a general scattering medium where $\sigma \neq 0$. The idea is to treat $\mathcal{X}_{a,\sigma}$ as a perturbation of the attenuated X-ray transform $\mathcal{X}_{a,0}$. Specifically, resolvent identities show that [SU08]

$$\mathcal{X}_{a,\sigma} = R_{+} T_{a}^{-1} + R_{+} T_{a}^{-1} K T_{a}^{-1} (I - T_{a}^{-1} K)^{-1}. \tag{8}$$

The first term $R_+T_a^{-1} = \mathcal{X}_{a,0}$ is just the attenuated X-ray transform, which is known to be invertible. Therefore, applying $\mathcal{X}_{a,0}^{-1}$ yields

$$\mathcal{X}_{a,0}^{-1}\mathcal{X}_{a,\sigma}f = [I + \underbrace{\mathcal{X}_{a,0}^{-1}R_{+}T_{a}^{-1}KT_{a}^{-1}(I - T_{a}^{-1}K)^{-1}}_{:=S}]f.$$

We now view the operator S as a perturbation to the identity. If the operator I + S is invertible by Neumann series (which holds, for example, if σ is sufficiently small so that S becomes a contraction [BT07]), we obtain

$$f = \sum_{j=0}^{\infty} (-1)^{j} S^{j} \mathcal{X}_{a,0}^{-1} \mathcal{X}_{a,\sigma} f.$$

This is an explicit inversion formula that recovers the bioluminescent source f from the BLT data $\mathcal{X}_{a,\sigma}f$. It is worth noting that the Neumann series is not the sole method for inversion. For example, [SU08] demonstrates that S is a compact operator for an open and dense subset of (a,k), leading to a Fredholm-type inversion. Moreover, convexification approaches [SKN19] and Fourier methods [FST20] have also been developed in addition to the perturbation arguments.

While the inversion holds mathematical validity, the illposedness remains due to the application of the unbounded operator $\mathcal{X}_{a,0}^{-1}$ to the BLT data. This is an inherent issue of the inverse problem. Indeed, the decomposition (8) indicates that the BLT data is dominated by the attenuated X-ray transform if σ is sufficiently small. This integral transform is known to have a smoothing effect in the sense that $\mathcal{X}_{a,0}f$ has higher Sobolev regularity than f. From the pespective of imaging sciences, a smoothing

process usually averages pixel values (for example, $\mathcal{X}_{a,0}$ averages pixel values along lines) and blurs image features such as edges and corners. The resulting smoother data cannot adequately capture abrupt variations and fine-scale details, leading to a loss of information. From the pespective of Fourier analysis, abrupt variations and fine-scale details are contained in the high frequencies, yet a smoothing process tends to damp the high-frequency content of a function. As a result, any inversion strategy must amplify the high frequency content in order to recover a less smooth function. In the filtered back-projection, such amplification is implemented with the help of the Hilbert transform and differentiation. A clear limitation, as has been discerned from our examination of the filtered backprojection, is that the amplification inevitably intensifies noises of high frequency, making the reconstruction less stable and reliable.

Ill-posedness is ubiquitous in inverse problems, and various methods have been developed to mitigate it. A generic class of techniques is regularization. Regularization stabilizes solutions of ill-posed problems by incorporating prior knowledge about the solution into the mathematical formulation. The integration of prior knowledge is achieved by adding a penalty term to discourage unlikely or unrealistic solutions. Typical penalty terms include constraints on the solution, assumptions about its smoothness, or expectations regarding characteristics of the solution. This additional penalty contributes to a more wellposed problem, reducing sensitivity to noise and guiding the inversion process towards more stable solutions. The idea of regularization has also found broad applications in machine learning for model complexity reduction and overfitting prevention.

5. Related Topics

The preceding sections provide an overview of both the forward and inverse problems in BLT, with a concise presentation summarizing the main ideas and results. However, there are crucial topics that are not covered in the outline. In this section, we delve into three topics concerning simplification and generalization of the BLT model. These topics remain vibrant research areas and give rise to even more intriguing mathematical questions.

5.1. Diffusion approximation. The RTE provides an accurate modeling of light propagation when the transport mean free path of photons is at the same order as the characteristic length of the medium. Nevertheless, the mean free path of photons in biological tissue is typically much shorter than the characteristic length. Light propagation in biological tissue is thus predominantly governed by diffusion, allowing for an effective approximation of the RTE using a diffusion equation

$$-\nabla \cdot D\nabla \Phi + \alpha \Phi = f(x)$$

subject to a homogeneous Robin boundary condition [KS05]. Here $\Phi(x) \coloneqq \int_{\mathbb{S}^{n-1}} u(x,\theta) \, d\theta$ is the angularly-averaged radiance, D is the diffusion coefficient, and α is the absorption coefficient. The diffusion approximation is derived using the ansatz that the radiance is linear in the angular variable θ . The underlying rationale is that when the scattering is strong, the radiance is expect to have a relatively smooth isotropic distribution hence it suffices to retain only the first angular moment. Higher-order angular moments are neglected as they represent more-detailed, fine-grained angular variations. The BLT inverse problem using the diffusion approximation requires identification of the bioluminescent source f from the effective boundary data $\Phi|_{\partial\Omega}$.

The diffusion approximation offers remarkable advantages in terms of computational efficiency and simplicity. For instance, the 3D RTE depends on three spatial variables and two angular variables, making numerical computation prohibitively expensive due to its high dimensionality. In contrast, the 3D diffusion approximation is a standard second-order elliptic equation for which various fast numerical solvers are readily available. However, the diffusion approximation also suffers a clear weakness: the BLT inverse problem becomes under-determined as the unknown source f is a higher-dimensional object than the boundary data. For example, if γ is a smooth function compactly supported inside Ω , the two bioluminescent sources f and $(-\nabla \cdot D\nabla + \alpha)\chi + f$ generate two diffusion solutions Φ and $\Phi + \chi$ respectively, yet the resulting BLT data is identical since $\chi|_{\partial\Omega} = \partial_{\nu}\chi|_{\partial\Omega} = 0$. This lack of identifiability represents another form of ill-posedness that is quite common for inverse problems. The approach to address this challenge involves either incorporating additional data that offers complementary insights (see Section 5.2), or confining the source to a more restrictive class based on prior knowledge.

5.2. **Ultrasound modulated BLT**. In BLT, photons emitted from a bioluminescent source undergo significant scattering in biological tissue, which blurs directional information and makes it challenging to accurately locate the source. Consequently, conventional BLT often suffers from limited spatial resolution. An emerging approach to overcome this limitation, known as *Ultrasound Modulated BLT (UMBLT)*, integrates BLT with ultrasound modulation. In UMBLT, ultrasound waves are used to manipulate the optical properties of the medium. The frequencies in use are approximately 1–5 MHz, which provide a good compromise between axial resolution and penetration depth. The interaction of ultrasound with biological tissue alters the paths of the photons, leading to more controlled redirection and increased spatial resolution.

Asymptotic analysis [BS14, BCS16] shows that UMBLT by plane waves allows for the calculation of the following

function inside Ω :

$$H(x) \coloneqq \int_{\mathbb{S}^{n-1}} v(x,\theta)\theta \cdot \nabla u(x,\theta) \, d\theta \qquad x \in \Omega,$$

where v denotes a solution of the adjoint RTE. Ideally, one may think of ultrasound modulation as a probing method that enables "internal measurement" H inside the tissue, and the inverse problem in UMBLT seeks to invert the source-to-internal-data map $f \mapsto H$. This map is a continuous linear operator with a bounded inverse [BCS16, CYY21]. Therefore, the inverse problem with internal data becomes well-posed, in contrast to the ill-posed inverse problem in the conventional BLT. The well-posedness implies that a small amount of noise causes only a minor deviation from the true solution, enabling UMBLT to provide more precise identification of the bioluminescent source with superior spatial resolution.

5.3. Riemannian RTE. Biological tissues often have complex structures that cannot be effectively modeled by Euclidean geometry. For instance, the scattering and absorption coefficients in structured tissue may not only vary spatially but also depend on direction. In such cases, Riemannian geometry allows for the incorporation of directional information, providing a more comprehensive representation of the optical properties of tissues. The BLT formulation on an n-dimensional ($n \ge 2$) compact smooth Riemannian manifold with boundary (M, g) is given by the integro-differential equation on the unit sphere bundle SM:

$$Gu(x,\theta) + a(x)u(x,\theta)$$
$$-\sigma(x) \int_{S_x M} k(x,\theta,\theta')u(x,\theta') d\sigma_x(\theta') = f(x) \text{ on } SM$$

subject to the the boundary condition (2). Here, G is the geodesic vector field restricted to SM, S_xM is the fiber of SM over x, and $d\sigma_x$ is the volume form on S_xM induced by the metric g(x). In the Euclidean geometry, the geodesic vector field reduces to $G|_{SM} = \xi \cdot \nabla$ with $|\xi| = 1$, agreeing with the RTE in (1). The solution is known to exist under sub-critical conditions [McD04, AY15], and the inverse problem seeks to recover the unknown source f from the outgoing radiation flux $u|_{\Gamma_x}$.

As in the Euclidean case, the crucial step for solving the inverse problem is to understand the non-scattering scenario k=0, then the general scenario can be handled using a similar perturbation argument as in Section 4.2. When k=0, the BLT data is

$$\mathcal{X}^{M}_{a,0}f(x,\theta) \coloneqq \int_{-\tau_{-}(x,\theta)}^{0} e^{\int_{-t}^{0} a(\gamma_{x,\theta}(t)) \, ds} f(\gamma_{x,\theta}(t)) \, dt$$

for $(x, \theta) \in \Gamma_+$, where $\gamma_{x,\theta}$ is the maximal geodesic with the initial conditions $\gamma_{x,\theta}(0) = x$ and $\dot{\gamma}_{x,\theta}(0) = \theta$. This is another integral transform where the integration is over

all geodesics with exponentially-weighted attenuation. It is the Riemannian counterpart of the attenuated Radon transform, known as the attenuated geodesic X-ray transform. When a=0, $\mathcal{X}_{a,0}^{M}$ is simply the geodesic X-ray transform. The invertibility of $\mathcal{X}_{a,0}^{M}$ is complicted by the geometry

The invertibility of $\mathcal{X}_{a,0}^{M}$ is complicted by the geometry of the manifold. For example, if the manifold contains maximal geodesics that cannot reach the boundary in a finite time, $\mathcal{X}_{a,0}^{M}$ clearly does not see the integration of f over such geodesics. A manifold is said to be *non-trapping* if no such geodesics exists. The study of $\mathcal{X}_{a,0}^{M}$ is better suited for a non-trapping manifold that has a strictly convex boundary (in the sense that the second fundamental form on ∂M is strictly positive), as Γ_{+} gives a convenient parameterization of all the maximal geodesics in this case. The geodesic X-ray transform and attenuated geodesic X-ray transforms for functions, or more broadly for symmetric tensor fields, remain vibrant research topics in integral geometry, geometric inverse problems and imaging sciences [Sha94].

6. Conclusion

The inverse problem in BLT encompasses numerous fascinating mathematical questions related to differential equations, integral geometry, and Fourier analysis, with vibrant research continually unfolding in this area. This essay provides only a glimpse into the extensive landscape of inverse problems within BLT. The perspective presented here is just one of many approaches to address these challenges, and the references provided are by no means exhaustive. The primary goal of this essay is to offer an introduction to this fascinating field and to outline some interesting mathematics in imaging sciences, with the hope of sparking the interest of junior researchers and inspiring their future contributions.

ACKNOWLEDGMENT. The author thanks Professor Gunther Uhlmann for helpful discussion. The article is based upon work supported by NSF CAREER Award DMS-2237534, NSF grants DMS-2006881, DMS-2220373, and NIH grant R03-EB033521.

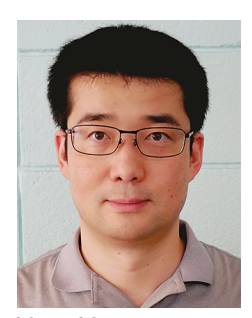
References

[Ago98] Valeri Agoshkov, Boundary value problems for transport equations, Modeling and Simulation in Science, Engineering and Technology, Birkhäuser Boston, Inc., Boston, MA, 1998, DOI 10.1007/978-1-4612-1994-1. MR1638817

[ABK97] È. V. Arbuzov, A. L. Bukhgeĭm, and S. G. Kazantsev, Two-dimensional problems in tomography, and the theory of A-analytic functions (Russian, with Russian summary), Algebra, geometry, analysis and mathematical physics (Russian) (Novosibirsk, 1996), Izdat. Ross. Akad. Nauk Sib. Otd. Inst. Mat., Novosibirsk, 1997, pp. 6–20, 189. MR1624170

- [AY15] Yernat M. Assylbekov and Yang Yang, An inverse radiative transfer in refractive media equipped with a magnetic field, J. Geom. Anal. 25 (2015), no. 4, 2148–2184, DOI 10.1007/s12220-014-9507-0. MR3427119
- [BCS16] Guillaume Bal, Francis J. Chung, and John C. Schotland, *Ultrasound modulated bioluminescence tomography and controllability of the radiative transport equation*, SIAM J. Math. Anal. 48 (2016), no. 2, 1332–1347, DOI 10.1137/15M1026262. MR3483159
- [BS14] Guillaume Bal and John C Schotland, *Ultrasound-modulated bioluminescence tomography*, Physical Review E 89 (2014), no. 3, 031201, https://doi.org/10.1103/PhysRevE.89.031201.
- [BT07] Guillaume Bal and Alexandru Tamasan, Inverse source problems in transport equations, SIAM J. Math. Anal. 39 (2007), no. 1, 57-76, https://doi.org/10.1137 /050647177. MR2318375
- [CS99] Mourad Choulli and Plamen Stefanov, An inverse boundary value problem for the stationary transport equation, Osaka J. Math. 36 (1999), no. 1, 87–104, http:// projecteuclid.org/euclid.ojm/1200788449. MR1670750
- [CYY21] Francis Chung, Tianyu Yang, and Yang Yang, *Ultrasound modulated bioluminescence tomography with a single optical measurement*, Inverse Problems 37 (2021), no. 1, Paper No. 015004, 19, DOI 10.1088/1361-6420/abc8aa. MR4191620
- [Eps08] Charles L. Epstein, Introduction to the mathematics of medical imaging, 2nd ed., Society for Industrial and Applied Mathematics (SIAM), Philadelphia, PA, 2008, DOI 10.1137/1.9780898717792. MR2378706
- [FS05] A. S. Fokas and L.-Y. Sung, Generalized Fourier transforms, their nonlinearization and the imaging of the brain, Notices Amer. Math. Soc. 52 (2005), no. 10, 1178–1192. MR2186901
- [FST20] Hiroshi Fujiwara, Kamran Sadiq, and Alexandru Tamasan, A Fourier approach to the inverse source problem in an absorbing and anisotropic scattering medium, Inverse Problems **36** (2020), no. 1, 015005, 33, DOI 10.1088/1361-6420/ab4d98. MR4047905
- [KS05] Jari Kaipio and Erkki Somersalo, *Statistical and computational inverse problems*, Applied Mathematical Sciences, vol. 160, Springer-Verlag, New York, 2005. MR2102218
- [McD04] Stephen R. McDowall, An inverse problem for the transport equation in the presence of a Riemannian metric, Pacific J. Math. 216 (2004), no. 2, 303–326, DOI 10.2140/pjm.2004.216.303. MR2094548
- [Nat01] F. Natterer, The mathematics of computerized tomography, Classics in Applied Mathematics, vol. 32, Society for Industrial and Applied Mathematics (SIAM), Philadelphia, PA, 2001. Reprint of the 1986 original, DOI 10.1137/1.9780898719284. MR1847845
- [Nov02] Roman G. Novikov, An inversion formula for the attenuated X-ray transformation, Ark. Mat. 40 (2002), no. 1, 145–167, DOI 10.1007/BF02384507. MR1948891
- [Sha94] V. A. Sharafutdinov, Integral geometry of tensor fields, Inverse and Ill-posed Problems Series, VSP, Utrecht, 1994, DOI 10.1515/9783110900095. MR1374572

- [SKN19] Alexey V. Smirnov, Michael V. Klibanov, and Loc H. Nguyen, On an inverse source problem for the full radiative transfer equation with incomplete data, SIAM J. Sci. Comput. 41 (2019), no. 5, B929–B952, DOI 10.1137/19M1253605. MR4002730
- [SU08] Plamen Stefanov and Gunther Uhlmann, *An inverse source problem in optical molecular imaging*, Anal. PDE **1** (2008), no. 1, 115–126, DOI 10.2140/apde.2008.1.115. MR2444095
- [WW12] Lihong V Wang and Hsin-i Wu, Biomedical optics: principles and imaging, John Wiley & Sons, 2012.



Yang Yang

Credits

Figure 1 is courtesy of kiwi616 via Pixabay.
Figure 2 is courtesy of EddieKphoto via Pixabay and NASA.
Figures 3–8 are courtesy of Yang Yang.
Photo of Yang Yang is courtesy of Guessy Wang.